

Nitroarene Reduction by a Virus Protein Cage Based Nanoreactor

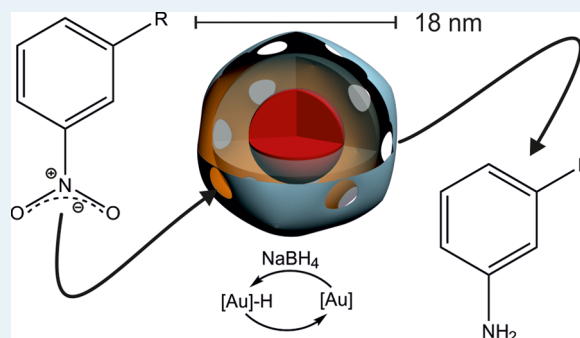
Aijie Liu,[†] Christoph H.-H. Traulsen,[†] and Jeroen J. L. M. Cornelissen*

Laboratory for Biomolecular Nanotechnology MESA+ Institute for Nanotechnology, University of Twente, P.O. Box 217, 7500 AE Enschede, The Netherlands

Supporting Information

ABSTRACT: Gold nanoparticles have recently gained attention as heterogeneous catalysts in a variety of industrially relevant processes. The catalytic activity of the particles is directly related to the available surface area, which increases with decreasing particle size. However, their stability in solution decreases along with the size, and surface modifications have to be carried out to enable efficient catalysis also for elongated reaction times. To prolong catalyst lifetime and to study the substrate selectivity, we encapsulated colloidal gold nanoparticles in cowpea chlorotic mottle virus cages and catalyzed the reduction of nitroarenes with different substituents. The reduction mechanism has been investigated carefully, revealing the reduction sequence nitro → hydroxylamine → amine to take place. The reduction rate is slowed by the introduction of the diffusion barrier imposed by the virus cage, and a nonconventional relation between electronic effects and reduction rate constants is reported that originates from the limited pore sizes and charged exterior/interior of the virus cage. Finally, a significantly increased stability of the hybrid nanoreactors and their recyclability are demonstrated.

KEYWORDS: virus-like particle, gold nanoparticle, catalysis, reduction, charge/size selectivity



INTRODUCTION

Sustainable chemistry is a major topic of current research in academia as well as in industry. Conventional approaches using (over-) stoichiometric amounts of reagents have been replaced by more efficient setups.¹ In this context, heterogeneous catalysts such as dispersed transition metals under an H₂ atmosphere have been applied to, for example, reduce ketones and aldehydes to alcohols. Transition metals such as palladium and platinum are used frequently, whereas gold as a bulk or microstructured material is considered to be inert.² However, decreasing the size of colloidal gold to the nanometer regime significantly increases its catalytic activity due to an increase of the surface available for adsorption/desorption processes of active species.³ Gold nanoparticle (AuNP) catalysts are especially interesting, because they enable mild reaction conditions and high chemoselectivity in reduction reactions.⁴ Among other reactions, the reduction of nitroarenes to the corresponding amines using AuNPs is of interest because of their toxicity and environmental concerns.^{5,6}

The reduction of 4-nitrophenol (4NP) with NaBH₄ as a hydride source is a model reaction to evaluate the performance of nanoparticle catalysts.⁷ One of the main problems using an AuNP catalyst is the inverse relation between catalyst activity and stability of the colloid.⁸ In order to circumvent this issue, gold nanoparticles can be stabilized by small molecules such as DMF⁹ or be deposited on colloids such as polymer brushes, core-shell particles, or similar carriers.^{10–14} Carriers such as mesoporous silica particles,^{15,16} tea-bag-like nanoparticle assemblies,¹⁷ amphiphilic nanoreactors,¹⁸ and polymeric

assemblies have been reported.¹⁷ Furthermore, gold nanotube membranes have been developed and successfully applied to the reduction of nitrophenol.¹⁹

In addition to synthetic carrier systems, natural assemblies such as protein cages as confined nanoreactors have promising features and recently gained attention in materials science.^{20–30} The main improvement in comparison to artificial carriers is their uniformity with respect to size and shape as well as the control of catalytic and substrate selectivity.^{31–34} In this context the application of nanoreactors for catalysis has been investigated by Douglas and co-workers taking advantage of encapsulated NADH oxidase for the production of hydrogen peroxide³⁵ and encapsulated TiO₂ particles for methylene blue decomposition.^{36,37} They demonstrated that enzymes encapsulated in the P22 cavity have a high efficiency of hydrogen production by taking advantage of the confined environment of viral cages.³⁸ Horse spleen apoferritin has been used by Shin et al. as a template for the synthesis of gold–silver alloys by diffusion based method and used as a catalyst for nitro-phenol reduction.³⁹ However, the size of ferritin cages does not expand beyond a diameter of 12 nm and the pore sizes are comparably small as well.⁴⁰ Thus, the particle size selection as well as possible size of substrates is limited, as has been investigated by Ueno et al.^{41,42} For further reading on the application of metal

Received: January 12, 2016

Revised: March 24, 2016

Published: March 29, 2016

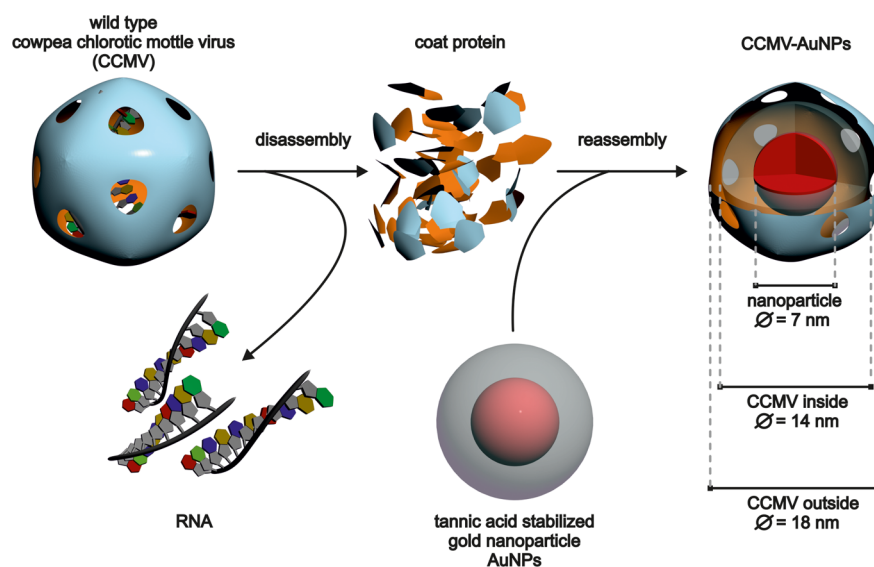


Figure 1. Preparation of gold nanoparticle loaded $T = 1$ cowpea chlorotic mottle virus cage.

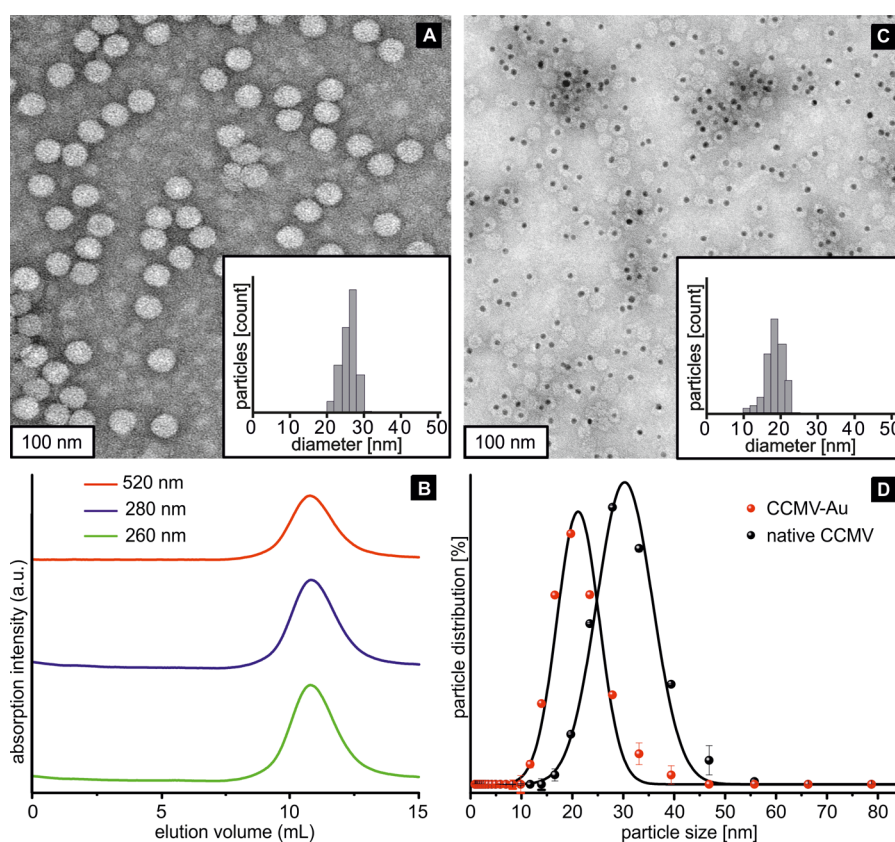


Figure 2. Analytical data of the native cowpea chlorotic mottle virus (CCMV) and the corresponding protein cage loaded with gold nanoparticles (CCMV-Au): (A) transmission electron microscopy (TEM) image of CCMV (inset: statistical analysis); (B) UV-vis absorption intensities of the main CCMV-Au fraction obtained by fast protein liquid chromatography (FPLC); (C) TEM image of CCMV-Au (inset: statistical analysis); (D) dynamic light scattering (DLS) data of CCMV (black dots) and CCMV-Au (red dots). Curves in (D) have been obtained by a Gaussian nonlinear fit of the data.

catalysts, we refer to a review by Hu et al. and references therein.⁴³

Protein cages such as the cowpea chlorotic mottle virus (CCMV) form monodisperse spheres in aqueous solutions.⁴⁴ The RNA cargo of CCMV can be removed by particle disassembly. Reassembly around a negatively charged template provides nanocarriers which can be used for drug delivery, for

example.⁴⁵ Decent knowledge about the properties, possible modifications, and applications of the CCMV protein cage have been acquired lately by us and others.^{45–55} In contrast to other available protein cages such as ferritin, CCMV can be assembled around a variety of templates with different sizes, forming highly monodisperse shapes enabling the investigation of a variety of heterogeneous catalysts.⁵⁶ The stimuli-responsive

reversible swelling of CCMV can be used to increase the pore size significantly.⁵⁷ Therefore, a broader range of catalysts can be encapsulated and numerous substrates can be investigated systematically.

In the present study we are aiming at a combination of the catalytic activity of gold nanoparticles (AuNPs) and the high biocompatibility and homogeneity of CCMV virus cages. Therefore, we encapsulated commercially available AuNPs into protein cages and catalyzed the reduction of differently substituted nitroarenes. The influence of the virus cage on the reduction has been investigated with respect to charge and size selectivity, yield, and stability.

RESULTS AND DISCUSSION

Nanoreactor Preparation. Wild-type CCMV was obtained from infected *Vigna unguiculata* plants (cowpea) and stored in virus buffer solution at 4 °C according to a well-established protocol.^{49,58} Disassembly and removal of the single-stranded RNA was carried out by dialysis against RNA buffer solution at pH 7.5 (see the Supporting Information).⁴⁴ Encapsulation of gold nanoparticles was carried out by injection of aqueous tannic acid stabilized gold nanoparticles into a solution of the disassembled coat protein subunits (Figure 1).⁴⁶

The commercially available anionic gold nanoparticles have a hydrodynamic diameter of $d = 7$ nm and template the formation of protein cages, likely of icosahedral nature.⁵⁹ Transmission electron spectroscopy (TEM) revealed a very regular shape and size of the isolated wild-type CCMV cages even after staining with uranyl acetate. The cages exhibit a mean diameter of $d = 26 \pm 2$ nm according to a statistical particle shape analysis (Figure 2A). Due to the drying and staining processes this value is slightly smaller than the $d = 28.6$ nm determined by Johnson and co-workers using X-ray diffraction.⁶⁰

Encapsulation of tannic acid stabilized gold nanoparticles form hybrid nanoparticles (CCMV-Au) which could be utilized as nanoreactors for the reduction of nitroarenes. Particle purification by fast liquid protein chromatography (FPLC) provides monodisperse virus cages which eluted at $V = 11$ mL. This fraction exhibits absorption bands at λ 520 nm resulting from the plasmon resonance of the encapsulated gold particles and bands at λ 260 and 280 nm which are assigned to the virus cages in accordance with one of our previous reports (Figure 2B).^{48,50} The reassembled AuNP-containing cages yield smaller $T = 1$ particles as determined using TEM. This is in accordance with results obtained by Bancroft and co-workers and Dragnea and co-workers and points to an assembly of 12 subunits each five-folded and positioned on the vertices of an icosahedron.⁶¹ The $T = 1$ cage in total consists of 60 coat identical protein subunits.^{59,61} Statistical analysis reveals a diameter for the hard core–soft shell particles of $d = 18 \pm 2$ nm (Figure 2C).

The encapsulated gold nanoparticles are clearly visible by areas of higher contrast inside the light particle cages and exhibit a measured diameter of $d = 6.0 \pm 1$ nm. The loading efficiency is 55% (123 out of the 222 detected virus cages are loaded with AuNP cargo). The origin of the limited loading efficiencies presumably originates from free tannic acid molecules in solution templating the protein cage formation as well. Nevertheless, most nanoparticles can be encapsulated (encapsulation efficiency up to 97%). The tannic acid loaded protein cages elute at the same volume as the gold encapsulated nanoparticles; thus separation is not possible by size exclusion chromatography. The size of the virus cages has been analyzed

using dynamic light scattering (Figure 2D). The resulting hydrodynamic radius of the native CCMV is $d = 30 \pm 1$ nm, whereas the nanoparticle loaded protein cage (CCMV-Au) exhibits a diameter of $d = 21 \pm 1$ nm. The size differences in comparison to TEM results are assigned to solvent effects; the solvent shell contributes to the particle velocity in solution.⁶² Due to the slightly anionic outer shell of the virus cage this effect is rather large; however, similar values have been obtained for $T = 1$ particles, which supports the formation of CCMV-Au nanoreactors.⁴⁷ The analytical data point to successful encapsulation of gold nanoparticles in CCMV based protein cages that show superior stability in aqueous solution (see below).

Mechanistic Investigation of the Nanoreactor-Catalyzed Reduction. The reduction of meta-substituted nitroarenes has been carried out under ambient conditions in a quartz glass cuvette. In order to evaluate the influence of the virus shell on nitroarenes with different charges and electronic structures, we chose 3-nitrobenzenesulfonate (NBS), 1-methyl-3-nitrobenzene (NTT), and *N,N,N*-trimethyl-1-(3-nitrophenyl)methanaminium (NTA) as substrates, introducing a negatively charged substituent with a $-I$ effect, a neutral species with a $+I$ effect, and a positively charged species with a $+I$ effect, respectively. Substitution at the meta position has been chosen in order to minimize electronic, especially mesomeric, effects which would further complicate the mechanistic analysis. We expect to see an influence of the charged substituents on the reduction reaction. The exterior of the protein cage is slightly negatively charged with a charge density of <0.1 e/nm², while the inner surface is highly positively charged with a charge density of >0.8 e/nm².^{63,64} This might induce a diffusion barrier and thus a charge selectivity. Furthermore, CCMV exhibits pores with a limited diameter, which is expected to have a retarding effect on the rates of reduction. The reductions have been carried out by adding the corresponding nitroarene to a solution of either gold nanoparticles or CCMV-Au nanoreactors before injecting sodium borohydride in the reaction container. The progress of the reactions was monitored by UV–vis-spectroscopy and mass spectrometry. Reaction yields were determined by HPLC.

The reduction of nitroarenes can be catalyzed by, for example, a dispersed transition metal, colloidal nanoparticles, a metal ion complex, or a hybrid assembly and starts with the addition of the hydride (source NaBH₄, for example) to the catalyst surface.^{65–69} According to the Langmuir–Hinshelwood model the nitro compound is adsorbed on the catalyst surface as well as the reactive hydride.⁷⁰ Detailed investigations have been carried out by Ballauf and co-workers, who used metallic nanoparticle/polymer brush assemblies for the reduction of nitrophenol and monitored the reaction kinetics by UV–vis spectroscopy.¹⁰ Three constants influence the reaction rates: (I) the surface reactivity of the bound components, (II) the adsorption constant of the hydride, and (III) the adsorption constant of the nitrophenol.¹⁰ The adsorption processes lead to an induction period without significant conversion before a quasi-stationary state is reached in which the slowest process is dominating the overall reaction rate constant. For very detailed investigations into the catalytic nitro reduction by nanoparticles, we refer to studies carried out by Yoshimura et al., Pal et al., and Peng and co-workers.^{71–73} The focus of the mechanistic investigations of the present study is on the molecular conversion processes and the influence of the protein cage shell on the reaction rate constants.

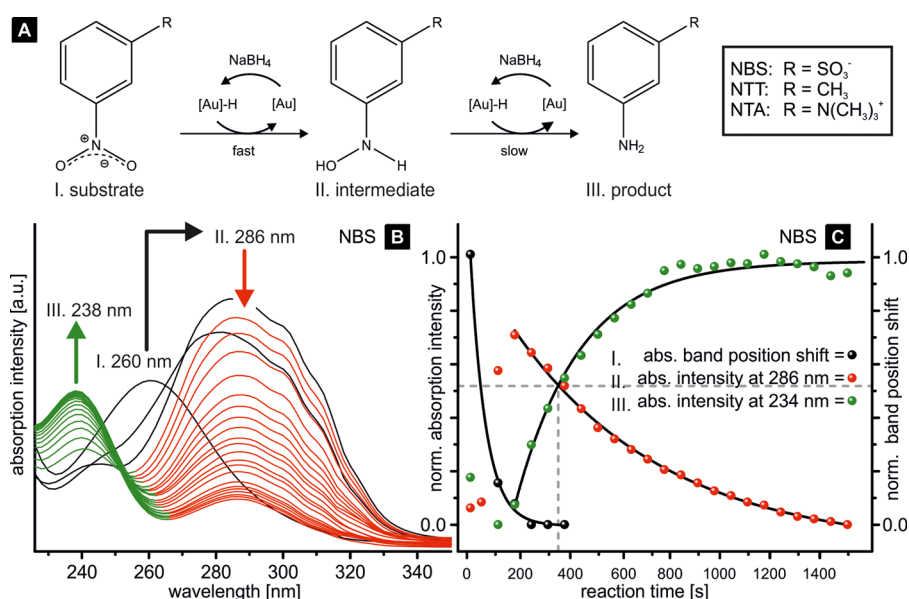


Figure 3. Reduction of meta-substituted nitroarenes with gold nanoparticle loaded $T = 1$ cowpea chlorotic mottle protein cage (CCMV-Au) nanoreactors in the presence of sodium borohydride: (A) reaction scheme; (B) UV-vis spectra of the reduction of 3-nitrobenzenesulfonate (NBS) to 3-aminobenzenesulfonate with sodium borohydride catalyzed by CCMV-Au; (C) plots of normalized absorption intensity (I) (intermediate and product) and absorption maximum shift (reactant). The $I = 100\%$ value of the intermediate is determined by nonlinear curve fitting (Figure S1 in the Supporting Information).

The progression of the reduction of nitroarenes catalyzed by titanium/gold nanoparticle assemblies has recently been investigated by Lykakis and co-workers.⁷⁴ They revealed hydroxylamines to be intermediately formed during the reduction. Accordingly, we propose a three-step reaction mechanism starting with the reduction of the nitro groups to the corresponding hydroxylamine. According to Lykakis, this step is fast in comparison to the subsequent reduction of the hydroxylamine to the final aminoarene (Figure 3A). The CCMV-Au catalyzed reduction of 3-nitrobenzenesulfonate (NBS) to 3-aminobenzenesulfonate was monitored by UV-vis spectroscopy, which provided mechanistic information in particular on the reduction sequence I \rightarrow II \rightarrow III: (I) the production of the intermediate hydroxylamine as represented by a shift of the main absorption at λ 260 nm to λ 286 nm (from the black to the red band in Figure 3B), (II) the consumption of this intermediate during amine formation as shown by a decrease of the λ 286 nm absorption band (decreasing signal in red in Figure 3B), and (III) the formation of the aminoarene as represented by the appearance and increase of a band at λ 238 nm (green signal in Figure 3B). Plots of the normalized absorption intensities at λ 260 and 286 nm and the shift of the absorption maximum lead to a reaction profile in agreement with a consecutive reaction (Figure 3C). The initial consumption of the starting material is fast (black dots in Figure 3C), whereas the consumption of the intermediately formed species is comparably slow (red dots in Figure 3C). Thus, the second reaction is slow, which can also be monitored by the increase of the product absorption band (green dots in Figure 3C), and consequently is the rate-determining step in the sequence. The half-life of the intermediate is reached at $t_{1/2} = 350$ s (dotted gray line).

To provide evidence for the presence of hydroxylamine, we investigated the reaction mixture of the NTA reduction after the addition of the hydride (Figure S3 in the Supporting Information). A solution of CCMV-Au and NTA was prepared

and after injection of the NaBH₄ solution the reaction mixture was transferred into a Hamiltonian syringe (250 μ L) and injected with a flow rate of 10 μ L/min into the ESI mass spectrometer, providing a stable spray. Ions were detected in the positive mode of the TOF analyzer. Each spectrum was produced out of 10 scans (1 s each). The starting material provides a single species at m/z 195.1 corresponding to the $[M]^+$ molecular ion of NTA. The expected intermediate 1-(3-(hydroxyamino)phenyl)-*N,N,N*-trimethylmethanaminium was identified by an ion peak at m/z 181.1 followed by the main product 1-(3-aminophenyl)-*N,N,N*-trimethylmethanaminium detected at m/z 165.1. After 21 min the MS spectrum revealed a domination of the product ion. Please note that the product/intermediate/reagent ratio does not necessarily correspond to the molar ratio in the reaction solution due to differences in ion formation in the ESI source.

Determination of the Reduction Rate Constants. The formation of the reactive $[Au]-H$ species is considered to be very fast and remains constant during the reaction due to the large excess of BH₄⁻ in the solution. According to the Langmuir-Hinshelwood model, the adsorption/desorption of the substrate and product on the catalysts surface significantly contributes to the reaction rate. The diffusion barrier introduced by the encapsulation of the gold nanoparticles inside the protein cage will change the overall rate constant of the differently charged nitroarenes. For the determination of these overall rate constants the starting period, without significant spectral changes, was not taken into account and the analysis was carried out in the quasi-steady-state regime in which the concentration of the substrate is significantly higher than the catalytic centers and does not change over time.

An indirect measure of the reactant concentration is the absorption band at λ 286 nm, which decreased upon conversion to the amine product. To properly analyze the reductions, we do need the initial absorption intensity of the intermediate A_0 . The direct measurement of this value is not possible due to the

initial induction period of the first reaction. Thus, the absorption intensity of the intermediate at $t = 0$ was determined by fitting an exponential decay to the absorption intensity at λ 286 nm and by locating the corresponding intercept. A_0 was used for the determination of the rate constants by plotting the logarithm of the obtained data versus the reaction time (Figure 4).

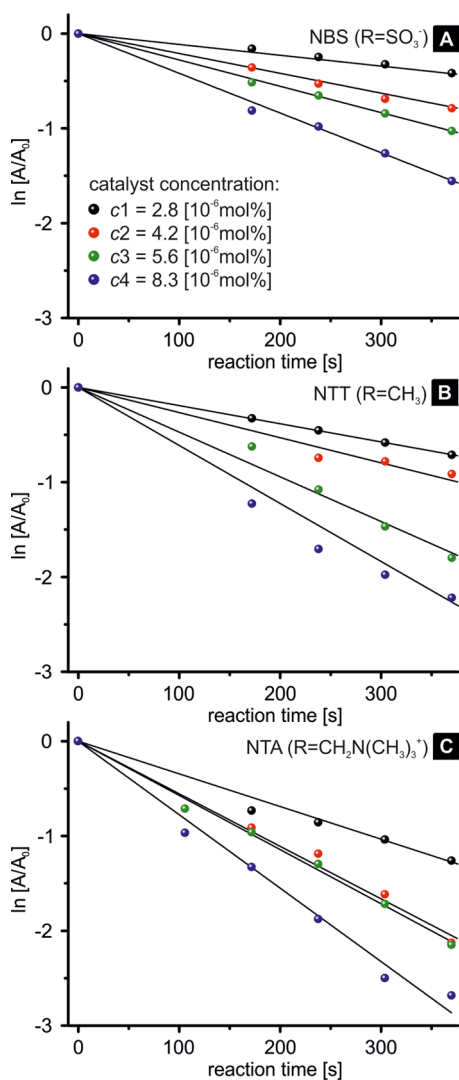


Figure 4. Plotted absorption maxima obtained during the reduction of (A) 3-nitrobenzenesulfonate (NBS), (B) 1-methyl-3-nitrobenzene (NTT), and (C) *N,N,N*-trimethyl-1-(3-nitrophenyl)methanaminium (NTA), with gold nanoparticle loaded $T = 1$ cowpea chlorotic mottle virus cage nanoreactors.

The reduction of NBS (Figure 4A), NTT (Figure 4B), and NTA (Figure 4C) was investigated. The concentration of the reactants was kept constant, whereas the amount of catalyst was systematically changed. The reactions were carried out using catalyst concentrations of $c \times 10^{-6}$ mol %. The fit of each concentration series is negative due to a decrease in the absorption intensity and an increase in the absolute slope with increasing catalyst concentration. According to the differential (eq 1) and the corresponding integrated (eq 2) rate laws, the slopes of these kinetic plots are equal to the rate constants of the reactions.

$$-\frac{d[A]}{dt} = k[A] \quad (1)$$

$$[A] = [A]_0 e^{-kt} \quad (2)$$

The determined rate fits with a first-order reaction, the rate constants of which are summarized in Table 1.

Table 1. Reduction Rate Constants (s^{-1}) of the Catalytic Reduction of Differently Substituted Nitroarenes

	NBS	NTT	NTA
c1	$(1.14 \times 10^{-3}) \pm (4.39 \times 10^{-5})$	$(1.93 \times 10^{-3}) \pm (2.01 \times 10^{-5})$	$(3.45 \times 10^{-3}) \pm (4.86 \times 10^{-5})$
c2	$(2.09 \times 10^{-3}) \pm (5.57 \times 10^{-5})$	$(2.65 \times 10^{-3}) \pm (9.75 \times 10^{-5})$	$(5.54 \times 10^{-3}) \pm (1.16 \times 10^{-4})$
c3	$(2.78 \times 10^{-3}) \pm (2.46 \times 10^{-5})$	$(4.72 \times 10^{-3}) \pm (1.29 \times 10^{-4})$	$(5.72 \times 10^{-3}) \pm (1.03 \times 10^{-4})$
c4	$(4.19 \times 10^{-3}) \pm (6.09 \times 10^{-5})$	$(6.12 \times 10^{-3}) \pm (2.57 \times 10^{-4})$	$(7.75 \times 10^{-3}) \pm (2.17 \times 10^{-4})$

In line with pseudo-first-order kinetics in the hydroxylammonium intermediate, a linear relation between the obtained rate constants and the initial catalyst concentration was found (Figure 5A).

For an interpretation of the influence of the virus protein cage on the reduction, three main effects have to be taken into account: (I) the electronic effects of the substituents on the aromatic core, (II) the diffusion barrier introduced by the negatively charged tannic acid layer, and (III) the diffusion

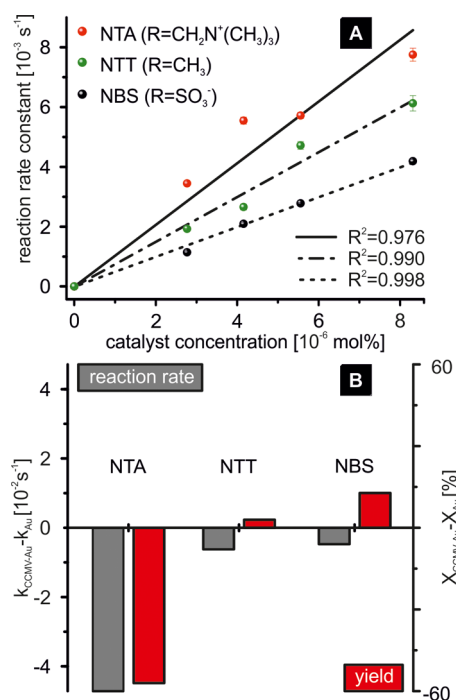


Figure 5. Kinetic investigation of the catalytic reduction of 3-nitrobenzenesulfonate (NBS), 1-methyl-3-nitrobenzene (NTT), and *N,N,N*-trimethyl-1-(3-nitrophenyl)methanaminium (NTA) with CCMV-Au nanoparticle loaded $T = 1$ cowpea chlorotic mottle virus cage nanoreactors: (A) reaction rate constants plotted versus the catalyst concentration; (B) reduction rate constants of CCMV-Au subtracted by the k values of reductions using tannic acid stabilized gold nanoparticles ($k_{\text{CCMV-Au}} - k_{\text{Au}}$; gray bar) and the corresponding yields of the reductions (red bar) determined by HPLC.

barrier introduced by the negatively (outside)/positively (inside) charged virus cage.

Electronic Effects of the Substituents on the Aromatic Core. Usually, substituents with electron-withdrawing substituents increase the reduction rates of nitroarenes with hydrides. The strongly electron withdrawing ($-M$, $-I$) nitro substituent is converted to an electron donating hydroxylamine and finally amine group ($+M$, $-I$). Consequently, the reduction should be fast for $R = \text{SO}_3^-$ and slower for $R = \text{CH}_3$, corresponding to NBS and NTT, respectively. Due to the benzylic position of the trimethylamine substituent the reduction of NTA is expected to be the fastest with $R = \text{CH}_2\text{N}^+(\text{CH}_3)_3$. The reduction rates are expected to follow the sequence $k_{\text{NTA}} > k_{\text{NBS}} > k_{\text{NTT}}$. Surprisingly, for the reduction carried out using bare tannic acid stabilized gold nanoparticles (AuNPs) the sequence is $k_{\text{NTA}} > k_{\text{NTT}} > k_{\text{NBS}}$ (Supporting Information). This behavior can only be explained by taking into account the influence of the negatively charged layer surrounding the gold nanoparticles.

Influence of the Negatively Charged AuNP Diffusion Barrier. The layer stabilizing the colloidal gold particles is composed of tannic acid. In addition to the steric stabilization of the nanoparticles, the phenol groups are partially deprotonated, increasing the water solubility. This charged shell is acting as a barrier for the diffusion of the negatively charged NBS and reduces the reduction rate significantly. The methyl substituent of NTT is not charged and is therefore less influenced by this layer. NTA is positively charged, which leads to an accelerated reduction of this substrate. To confirm the inversion in reaction rate trends, a Hammett plot of the reduction using bare gold nanoparticles (Figure S18 in the Supporting Information, σ_m values obtained from Hansch, Leo, and Taft)⁷⁵ was made, which does not yield a positive slope as is commonly observed for the reduction of nitroarenes using hydrides.⁷⁴

Influence of the Diffusion Barrier Introduced by the Negatively (Outside)/Positively (Inside) Charged Protein Cage. Only negatively charged cargos can be encapsulated in CCMV due to the positively charged arginine-rich motif of the coat protein (CP). The charge match between the cargo and the CPs is important for the capsid formation as well as the electrostatic interactions.⁵⁶ In order to evaluate the effect of the nanoparticle encapsulation on the reduction rate, we subtracted the obtained rate constants of the CCMV-Au catalyzed reduction by the AuNP-catalyzed reduction according to Figure 5B. All reduction rates are reduced by the introduction of the virus protein cage, as can be seen from the negative values (gray bars). The effect can be traced to the influence of the protein cage, because all other reaction conditions were kept constant. We assign this effect to a combination of steric hindrance and charge repulsion because it is most prominent for the positively charged substrate NTA. The substrates must pass the positively charged interior of the coat protein to access the gold catalyst. The related electrostatic explains the differences in reduction rates. In combination with the slight enhancement of NBS (negatively charge) reduction, it seems that these charges play an important role.

The same trend is observed for the yield of reduction as determined by HPLC (Figure 5B, red bar), which in the case of the reduction of NTA is reduced from 99% to 42% (-57%) for bare AuNP and CCMV-Au catalysis, respectively. The yields of NBS and NTT reduction are increased by 13% and 3%, respectively. This is attributed to the increased stability of the

gold catalyst upon encapsulation, which is only important for prolonged reaction times.

Stability. The instability of colloidal micro- or nanoparticle catalysts can be a major problem in heterogeneous catalysis. The particles form clusters, crush out of solution, remain insoluble, and can no longer act as catalysts. Pristine tannic acid stabilized nanoparticles precipitate from aqueous solution already after several hours, forming a black precipitate (Figure 6A, left). In marked contrast, CCMV protein capped nanoparticles do not coagulate and remain stable in solution (Figure 6A, right).

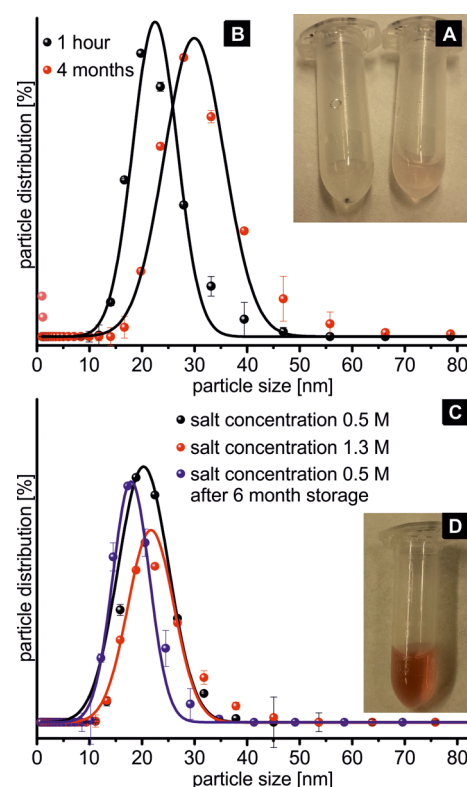


Figure 6. Stability of cowpea chlorotic mottle virus cages loaded with tannic acid stabilized gold nanoparticles (CCMV-Au). (A) optical image of pristine tannic acid capped nanoparticles (left) and virus cage encapsulated gold nanoparticles (right) after reaction; (B) dynamic light scattering (DLS) data obtained of CCMV-Au 1 hr after stopping the catalytic reaction (black dots) and 4 months after stopping the catalytic reaction (red dots), respectively (the observed light red data points have not been taken into account for Gaussian fit); (C) dynamic light scattering (DLS) data obtained from CCMV-Au nanoreactors in Tris-HCl buffered solutions with NaCl concentrations of 0.5 M NaCl (black dots) and 1.3 M NaCl (red dots) 1 h after preparation and with 0.5 M NaCl after 6 months of storage (no particle degeneration is observed); (D) optical image of virus cage encapsulated gold nanoparticles (right) in 0.5 M NaCl after 6 months of storage.

DLS investigations reveal the high stability of protein based colloidal gold nanoreactors (Figure 6C); CCMV-Au nanoreactors remain a stable dispersion after 4 months, although a slight increase in particle diameter is observed in Figure 6B (red dots). The reason for this increase is currently under further investigation. The nanoreactors remain stable also in buffered solutions with a high salt concentration (Figure 6C). Usually, nanoparticles coagulate over time in high salt buffers.⁷⁶ Our CCMV-Au nanoreactors stay intact even after 6 months of

storage in Tris-HCl buffer solution with 0.5 M NaCl (Figure 6C,D).

Sustainability. To provide further evidence for the advantages of encapsulated AuNP, several reaction cycles were carried out. After each cycle the CCMV-Au nanoreactors were regained by centrifuge filtration and reused for the reduction of NTA (c3, Figures S19–S23 in the Supporting Information). No catalyst degeneration or particle coagulation is observed after four subsequent cycles. The corresponding reduction rate constants remain constant under the applied conditions (Table 2 and Figure S23).

Table 2. Reduction Rate Constants (s^{-1}) of the Catalytic Reduction of *N,N,N*-Trimethyl-1-(3-nitrophenyl)methanaminium (NTA) Performed with the Same (Recycled) CCMV-Au Nanoreactors

	NTA
recycled 0	$(5.70 \times 10^{-3}) \pm (92.54 \times 10^{-4})$
recycled 1	$(5.45 \times 10^{-3}) \pm (5.98 \times 10^{-4})$
recycled 2	$(6.64 \times 10^{-3}) \pm (2.41 \times 10^{-4})$
recycled 3	$(6.90 \times 10^{-3}) \pm (3.37 \times 10^{-4})$

The nanoreactors can also be disassembled and reassembled, suggesting straightforward recycling of the gold particles. We carried out a reduction reaction, separated the product, and subsequently disassembled the CCMV-Au particles. The capsid protein and the tannic acid stabilized gold nanoparticle were reassembled. TEM investigation of the reassembled CCMV-Au revealed successful particle re-encapsulation; the loading efficiency decreased to 38% (44 of 115 CCMV loaded with gold nanoparticles), likely because of precipitation of AuNPs or formation of additional capsids. However, the particles could be used afterward for further reduction reactions (Figure S24 in the Supporting Information).

CONCLUSION

CCMV-Au nanoreactors were synthesized by loading cowpea chlorotic mottle virus cages with tannic acid stabilized gold nanoparticles. The particles were used to catalyze the reduction of nitroarenes with different substituents, which was monitored using UV-vis spectroscopy and MS spectrometry. The reaction sequence was initiated with a short induction period followed by the fast conversion of the nitro group to a hydroxylamine and a final reaction step to form the amine product, which was relatively slow.

The reduction of three differently meta substituted nitroarenes has been investigated: $R = SO_3^-, CH_3, CH_2N^+(CH_3)_3$. The rate constants of all of the reductions depend linearly on the catalyst concentration, pointing to pseudo-first-order kinetics where $k_{NTA} > k_{NTT} > k_{NBS}$. This sequence is attributed to the electrostatic barrier of the negatively charged tannic acid layer encountered inside the oppositely charged protein cage interior. The virus cage introduces an additional diffusion barrier, which significantly reduces the reduction rate of the positively charged NTA. The retarding effect of the barrier is traced to the steric hindrance imposed by the capsid as well as the positively charged interior of the cage.

Nanoreactors based on the CCMV protein cage and a gold nanoparticle have been successfully constructed and are active in the catalytic reduction of nitroarenes. These results show that protein cages assist in improving the stability of the catalytic nanoparticles, eventually leading to a longer lifetime

and therewith an increased conversion, despite the reduced reaction rates. Furthermore, the catalytic nanoparticles can be reused after isolation and re-encapsulation in the protein cage or isolated as intact nanoreactors and reused for catalytic reduction. The highly organized supramolecular assembly of virus capsid proteins around catalytically active nanoparticles opens the way to influence reactivity and has the potential to control substrate selectivity on the basis of charge and size.⁴¹

ASSOCIATED CONTENT

Supporting Information

The Supporting Information is available free of charge on the ACS Publications website at DOI: 10.1021/acscatal.6b00106.

Details on the materials, methods, instrumentation, and data processing as well as additional analytical data (PDF)

AUTHOR INFORMATION

Corresponding Author

*E-mail for J.J.L.M.C.: J.J.L.M.Cornelissen@utwente.nl.

Author Contributions

†These authors contributed equally.

Notes

The authors declare no competing financial interest.

ACKNOWLEDGMENTS

This research forms part of the research program of the Dutch Polymer Institute (DPI), Project #777t (DPI, P.O. Box 902, 5600 AX Eindhoven, The Netherlands), and financial support from the ERC (Consolidator Grant ProtCage #616907) is gratefully acknowledged.

REFERENCES

- Mitsudome, T.; Kaneda, K. *Green Chem.* **2013**, *15*, 2636–2654.
- Takale, B. S.; Bao, M.; Yamamoto, Y. *Org. Biomol. Chem.* **2014**, *12*, 2005–2027.
- Mikami, Y.; Noujima, A.; Mitsudome, T.; Mizugaki, T.; Jitsukawa, K.; Kaneda, K. *Chem. - Eur. J.* **2011**, *17*, 1768–1772.
- Chen, Y.; Qiu, J.; Wang, X.; Xiu, J. *J. Catal.* **2006**, *242*, 227–230.
- Corma, A.; Serna, P. *Science* **2006**, *313*, 332–334.
- Zhao, P.; Feng, X.; Huang, D.; Yang, G.; Astruc, D. *Coord. Chem. Rev.* **2015**, *287*, 114–136.
- Wunder, S.; Lu, Y.; Albrecht, M.; Ballauff, M. *ACS Catal.* **2011**, *1*, 908–916.
- Wu, S.; Dzubilla, J.; Kaiser, J.; Drechsler, M.; Guo, X.; Ballauff, M.; Lu, Y. *Angew. Chem., Int. Ed.* **2012**, *51*, 2229–2233.
- Liu, X.; Li, C.; Xu, J.; Lv, J.; Zhu, M.; Guo, Y.; Cui, S.; Liu, H.; Wang, S.; Li, Y. *J. Phys. Chem. C* **2008**, *112*, 10778–10783.
- Wunder, S.; Polzer, F.; Lu, Y.; Mei, Y.; Ballauff, M. *J. Phys. Chem. C* **2010**, *114*, 8814–8820.
- Liu, H.; Wang, J.; Feng, Z.; Lin, Y.; Zhang, L.; Su, D. *Small* **2015**, *11*, 5059–5064.
- Zhang, Y.; Xiang, S.; Zhou, Y.; Xu, Y.; Zhang, Z.; Sheng, X.; Wang, Q.; Zhang, C. *RSC Adv.* **2015**, *5*, 48187–48193.
- Bolisetty, S.; Arcari, M.; Adamcik, J.; Mezzenga, R. *Langmuir* **2015**, *31*, 13867–13873.
- Liu, G.; Wang, D.; Zhou, F.; Liu, W. *Small* **2015**, *11*, 2807–2816.
- Cao, Z.; Chen, H.; Zhu, S.; Chen, Z.; Xu, C.; Qi, D.; Ziener, U. *Colloids Surf., A* **2016**, *489*, 223–233.
- Lee, J.; Park, J. C.; Song, H. *Adv. Mater.* **2008**, *20*, 1523–1528.
- Mitschang, F.; Schmalz, H.; Agarwal, S.; Greiner, A. *Angew. Chem., Int. Ed.* **2014**, *53*, 4972–4975.

- (18) Zou, H.; Wang, R.; Dai, J.; Wang, Y.; Wang, X.; Zhang, Z.; Qiu, S. *Chem. Commun.* **2015**, *51*, 14601–14604.
- (19) Yu, Y.; Kant, K.; Shapter, J. G.; Addai-Mensah, J.; Losic, D. *Microporous Mesoporous Mater.* **2012**, *153*, 131–136.
- (20) Zhao, Y.; Sakai, F.; Su, L.; Liu, Y.; Wei, K.; Chen, G.; Jiang, M. *Adv. Mater.* **2013**, *25*, 5215–5256.
- (21) Zelzer, M.; Ulijn, R. V. *Chem. Soc. Rev.* **2010**, *39*, 3351–3357.
- (22) Patterson, D. P.; Prevelige, P. E.; Douglas, T. *ACS Nano* **2012**, *6*, 5000–5009.
- (23) Bode, S. A.; Minten, I. J.; Nolte, R. J. M.; Cornelissen, J. J. L. M. *Nanoscale* **2011**, *3*, 2376–2389.
- (24) Douglas, T.; Young, M. *Nature* **1998**, *393*, 152–155.
- (25) Ueno, T.; Suzuki, M.; Goto, T.; Matsumoto, T.; Nagayama, K.; Watanabe, Y. *Angew. Chem.* **2004**, *116*, 2581–2584.
- (26) Capehart, S. L.; Coyle, M. P.; Glasgow, J. E.; Francis, M. B. *J. Am. Chem. Soc.* **2013**, *135*, 3011–3016.
- (27) Wang, T.; Zhang, Z.; Gao, D.; Li, F.; Wei, H.; Liang, X.; Cui, Z.; Zhang, X.-E. *Nanoscale* **2011**, *3*, 4275–4282.
- (28) Loo, L.; Guenther, R. H.; Basnayake, V. R.; Lommel, S. A.; Franzen, S. *J. Am. Chem. Soc.* **2006**, *128*, 4502–4503.
- (29) Huang, X.; Bronstein, L. M.; Retrum, J.; Dufort, C.; Tsvetkova, I.; Aniyagei, S.; Stein, B.; Stucky, G.; McKenna, B.; Remmes, N.; Baxter, D.; Kao, C. C.; Dragnea, B. *Nano Lett.* **2007**, *7*, 2407–2416.
- (30) Sun, J.; DuFort, C.; Daniel, M.-C.; Murali, A.; Chen, C.; Gopinath, K.; Stein, B.; De, M.; Rotello, V. M.; Holzenburg, A.; Kao, C. C.; Dragnea, B. *Proc. Natl. Acad. Sci. U. S. A.* **2007**, *104*, 1354–1359.
- (31) van Rijn, P.; Boker, A. *J. Mater. Chem.* **2011**, *21*, 16735–16747.
- (32) Jutz, G.; van Rijn, P.; Santos Miranda, B.; Böker, A. *Chem. Rev.* **2015**, *115*, 1653–1701.
- (33) Culver, J. N.; Brown, A. D.; Zang, F.; Gnerlich, M.; Gerasopoulos, K.; Ghodssi, R. *Virology* **2015**, *479–480*, 200–212.
- (34) Slocik, J. M.; Naik, R. R.; Stone, M. O.; Wright, D. W. *J. Mater. Chem.* **2005**, *15*, 749–753.
- (35) Patterson, D. P.; McCoy, K.; Fijen, C.; Douglas, T. *J. Mater. Chem. B* **2014**, *2*, 5948–5951.
- (36) Bedwell, G. J.; Zhou, Z.; Uchida, M.; Douglas, T.; Gupta, A.; Prevelige, P. E. *Biomacromolecules* **2015**, *16*, 214–218.
- (37) Klem, M. T.; Young, M.; Douglas, T. *J. Mater. Chem.* **2008**, *18*, 3821–3823.
- (38) Jordan, P. C.; Patterson, D. P.; Saboda, K. N.; Edwards, E. J.; Miettinen, H. M.; Basu, G.; Thielges, M. C.; Douglas, T. *Nat. Chem.* **2016**, *8*, 179–185.
- (39) Shin, Y.; Dohnalkova, A.; Lin, Y. *J. Phys. Chem. C* **2010**, *114*, 5985–5989.
- (40) Jutz, G.; van Rijn, P.; Santos Miranda, B.; Böker, A. *Chem. Rev.* **2015**, *115*, 1653–1701.
- (41) Ueno, T.; Suzuki, M.; Goto, T.; Matsumoto, T.; Nagayama, K.; Watanabe, Y. *Angew. Chem., Int. Ed.* **2004**, *43*, 2527–2530.
- (42) Maity, B.; Fujita, K.; Ueno, T. *Curr. Opin. Chem. Biol.* **2015**, *25*, 88–97.
- (43) Hu, H.; Xin, J. H.; Hu, H.; Wang, X.; Miao, D.; Liu, Y. *J. Mater. Chem. A* **2015**, *3*, 11157–11182.
- (44) Verduin, B. J. M. *FEBS Lett.* **1974**, *45*, 50–54.
- (45) Soto, C. M.; Ratna, B. R. *Curr. Opin. Biotechnol.* **2010**, *21*, 426–438.
- (46) Verwegen, M.; Cornelissen, J. J. L. M. *Macromol. Biosci.* **2015**, *15*, 98–110.
- (47) Sikkema, F. D.; Comellas-Aragones, M.; Fokkink, R. G.; Verduin, B. J. M.; Cornelissen, J. J. L. M.; Nolte, R. J. M. *Org. Biomol. Chem.* **2007**, *5*, 54–57.
- (48) de la Escosura, A.; Verwegen, M.; Sikkema, F. D.; Comellas-Aragones, M.; Kirilyuk, A.; Rasing, T.; Nolte, R. J. M.; Cornelissen, J. J. L. M. *Chem. Commun.* **2008**, 1542–1544.
- (49) Comellas-Aragones, M.; Engelkamp, H.; Claessen, V. I.; Sommerdijk, N. A. J. M.; Rowan, A. E.; Christianen, P. C. M.; Maan, J. C.; Verduin, B. J. M.; Cornelissen, J. J. L. M.; Nolte, R. J. M. *Nat. Nanotechnol.* **2007**, *2*, 635–639.
- (50) Hommersom, C. A.; Matt, B.; van der Ham, A.; Cornelissen, J. J. L. M.; Katsonis, N. *Org. Biomol. Chem.* **2014**, *12*, 4065–4069.
- (51) Minten, I. J.; Hendriks, L. J. A.; Nolte, R. J. M.; Cornelissen, J. J. L. M. *J. Am. Chem. Soc.* **2009**, *131*, 17771–17773.
- (52) Garmann, R. F.; Sportsman, R.; Beren, C.; Manoharan, V. N.; Knobler, C. M.; Gelbart, W. M. *J. Am. Chem. Soc.* **2015**, *137*, 7584–7587.
- (53) Allen, M.; Bulte, J. W. M.; Liepold, L.; Basu, G.; Zywicke, H. A.; Frank, J. A.; Young, M.; Douglas, T. *Magn. Reson. Med.* **2005**, *54*, 807–812.
- (54) Suci, P. A.; Klem, M. T.; Arce, F. T.; Douglas, T.; Young, M. *Langmuir* **2006**, *22*, 8891–8896.
- (55) Cadena-Nava, R. D.; Hu, Y.; Garmann, R. F.; Ng, B.; Zelikin, A. N.; Knobler, C. M.; Gelbart, W. M. *J. Phys. Chem. B* **2011**, *115*, 2386–2391.
- (56) Garmann, R. F.; Comas-Garcia, M.; Knobler, C. M.; Gelbart, W. M. *Acc. Chem. Res.* **2016**, *49*, 48–55.
- (57) Renggli, K.; Baumann, P.; Langowska, K.; Onaca, O.; Bruns, N.; Meier, W. *Adv. Funct. Mater.* **2011**, *21*, 1241–1259.
- (58) Verduin, B. J. M. *J. Gen. Virol.* **1978**, *39*, 131–147.
- (59) Sun, J.; DuFort, C.; Daniel, M.-C.; Murali, A.; Chen, C.; Gopinath, K.; Stein, B.; De, M.; Rotello, V. M.; Holzenburg, A.; Kao, C. C.; Dragnea, B. *Proc. Natl. Acad. Sci. U. S. A.* **2007**, *104*, 1354–1359.
- (60) Speir, J. A.; Munshi, S.; Wang, G.; Baker, T. S.; Johnson, J. E. *Structure* **1995**, *3*, 63–78.
- (61) Bancroft, J. B.; Hills, G. J.; Markham, R. *Virology* **1967**, *31*, 354–379.
- (62) Traulsen, C. H. H.; Kunz, V.; Heinrich, T.; Richter, S.; Holzweber, M.; Schulz, A.; von Krbek, L. K. S.; Scheuschner, U. T. J.; Poppenberg, J.; Unger, W. E. S.; Schalley, C. A. *Langmuir* **2013**, *29*, 14284–14292.
- (63) Prinsen, P.; van der Schoot, P.; Gelbart, W. M.; Knobler, C. M. *J. Phys. Chem. B* **2010**, *114*, 5522–5533.
- (64) Konecny, R.; Trylska, J.; Tama, F.; Zhang, D.; Baker, N. A.; Brooks, C. L.; McCammon, J. A. *Biopolymers* **2006**, *82*, 106–120.
- (65) Downing, R. S.; Kunkeler, P. J.; van Bekkum, H. *Catal. Today* **1997**, *37*, 121–136.
- (66) Layek, K.; Kantam, M. L.; Shirai, M.; Nishio-Hamane, D.; Sasaki, T.; Maheswaran, H. *Green Chem.* **2012**, *14*, 3164–3174.
- (67) Wienhöfer, G.; Sorribes, I.; Boddien, A.; Westerhaus, F.; Junge, K.; Junge, H.; Llusar, R.; Beller, M. *J. Am. Chem. Soc.* **2011**, *133*, 12875–12879.
- (68) García, N.; García-García, P.; Fernández-Rodríguez, M. A.; Rubio, R.; Pedrosa, M. R.; Arnáiz, F. J.; Sanz, R. *Adv. Synth. Catal.* **2012**, *354*, 321–327.
- (69) Pozun, Z. D.; Rodenbusch, S. E.; Keller, E.; Tran, K.; Tang, W.; Stevenson, K. J.; Henkelman, G. *J. Phys. Chem. C* **2013**, *117*, 7598–7604.
- (70) Xu, W.; Kong, J. S.; Chen, P. *J. Phys. Chem. C* **2009**, *113*, 2393–2404.
- (71) Esumi, K.; Isono, R.; Yoshimura, T. *Langmuir* **2004**, *20*, 237–243.
- (72) Saha, S.; Pal, A.; Kundu, S.; Basu, S.; Pal, T. *Langmuir* **2010**, *26*, 2885–2893.
- (73) Gao, Y.; Ding, X.; Zheng, Z.; Cheng, X.; Peng, Y. *Chem. Commun.* **2007**, 3720–3722.
- (74) Fountoulaki, S.; Daikopoulou, V.; Gkizis, P. L.; Tamiolakis, I.; Armatas, G. S.; Lykakis, I. N. *ACS Catal.* **2014**, *4*, 3504–3511.
- (75) Hansch, C.; Leo, A.; Taft, R. W. *Chem. Rev.* **1991**, *91*, 165–195.
- (76) Gill, R.; Goeken, K.; Subramaniam, V. *Chem. Commun.* **2013**, *49*, 11400–11402.